Understanding the electronic structure, optical, and vibrational properties of the Fe_8Br_8 single-molecule magnet

Tunna Baruah
Department of Physics, Georgetown University, 37th and O Streets, Washington, DC 20057, USA and Center for Computational Materials Science, Code 6390, Naval Research Laboratory, 4555 Overlook Avenue, Washington, DC 20375-5000, USA

Jens Kortus
Max Planck Institut für Festkörperforschung, Heisenbergstr. 1, D-70569 Stuttgart, Germany

Mark R. Pederson
Center for Computational Materials Science, Code 6390, Naval Research Laboratory, 4555 Overlook Avenue Washington, DC 20375-5000, USA

Roman Wesołowski and Jason T. Haraldsen
Department of Physics, University of Tennessee, Knoxville, Tennessee 37996 USA

Janice L. Musfeldt
Department of Chemistry, University of Tennessee, Knoxville, Tennessee 37996 USA

J. Micah North, David Zipse, and Naresh S. Dalal
Department of Chemistry and Biochemistry, and NHMFL, Florida State University, Tallahassee, Florida 32306 USA
(Received 5 May 2004; published 8 December 2004)

We present the results of our all-electron density functional calculation on the electronic structure and optical properties of $[Fe_8O_2(OH)_{12}(C_6H_{15}N_3)_6Br_6]^{2+}$, the functional building block of the $[(C_6H_{15}N_3)_6Fe_8(\mu_3-O)_2(\mu_2-OH)_{12}]Br_7(H_2O)Br.8H_2O$ single-molecule magnet. The calculated results are compared with the experimentally measured optical spectrum, and the primary features of the excitations are assigned. Excellent agreement is obtained. The calculated spin minority gap is 0.23 eV, the spin majority gap is 0.54 eV, and the spin majority to minority gap is 0.15 eV. Notably, the low-energy spin minority gap is not a dipole-allowed excitation. Experimentally, we find that $[(C_6H_{15}N_3)_6Fe_8(\mu_3-O)_2(\mu_2-OH)_{12}]Br_7(H_2O)Br.8H_2O$ is a semiconductor, with a dipole-allowed optical gap of approximately 0.6 eV (peak position at ~0.9 eV) and an additional optically observable electronic excitation centered at 0.4 eV. The latter feature is weak and broad, with superimposed (C—H, N—H, and O—H) vibrational structure. We suggest that the 0.4 eV peak in the optical conductivity may be attributable to the spin majority highest occupied molecular orbital to spin minority lowest unoccupied molecular orbital excitation, activated by inclusion of spin-orbit coupling, which mixes states of different symmetry and spin. Overall, we find that the low-energy excitations are dominated by Fe $d \rightarrow$ Fe d interionic excitations and that the dipole-allowed excitations involve antiferromagnetically coupled pairs of Fe ions. At higher energy, the features are primarily due to O $p \rightarrow$ Fe d charge transfer transitions. A discussion of the vibrational properties is also included along with an analysis of how the electronic structure results support reduced moments on the minority spin Fe ions.

DOI: 10.1103/PhysRevB.70.214410 PACS number(s): 75.50.Xx, 75.30.Gw, 75.45.+j, 75.30.Et

I. INTRODUCTION

Magnetic materials play a very important role in today's information technology. In order to increase the capacity for information storage, the system size of the storage devices must be decreased, motivating the transition from bulk matter to nanoscale molecular and cluster-based functional units. Single molecule magnets seem promising candidates for such applications.[1] They are also interesting due to the phenomenon of quantum tunneling of magnetization at low temperature.[2] Magnetic molecular clusters such as the manganese-oxo cluster with acetate ligands (Mn_{12}-acetate)[1] or the octanuclear iron(III) oxo-hydroxo cluster (Fe_8Br_8)[3,4] are probably the most widely studied materials for which magnetic quantum tunneling has been observed.[5–8] These molecular clusters are particularly interesting[9–15] because conventional chemical synthesis allows for regularly assembled crystals in which all building block molecules are identical and very often have the same orientation.

The properties of a nanoscale system of coupled spins depend on the strength of the exchange parameters and also on the spin-orbit coupling. It is therefore essential to understand its electronic structure in order to correctly predict the corresponding magnetic behavior. At the same time, calculations on correlated systems present a challenge to mean-field frameworks such as density-functional theory (DFT)[16] because of the difficulty in accounting for strong ligand-metal interactions. Earlier DFT calculations of magnetic anisotro-

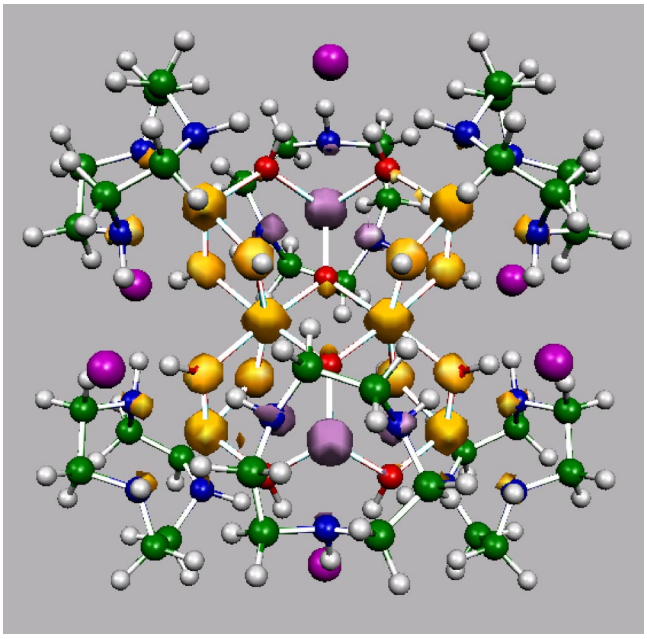

FIG. 1. The optimized geometry of the $[Fe_8O_2(OH)_{12}(C_6H_{15}N_3)_6Br_6]^{2+}$ cluster. The large balls show isosurfaces of the spin density at 0.0005 $\mu_B/Å^3$. The orange surface shows the majority spin while the purple surface shows the minority spin. The spin density is seen on some of the bridging oxygens.

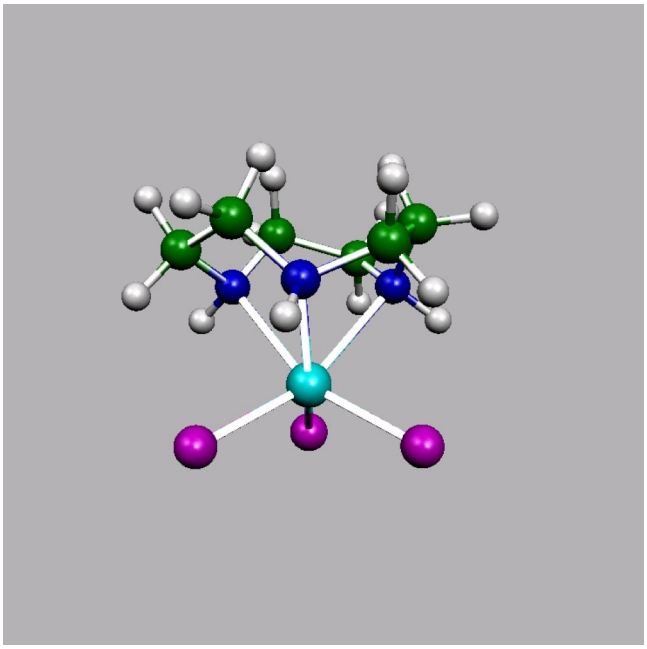

FIG. 2. The optimized geometry of the $[FeCl_3$-(tacn)] molecule.

pies on a wide variety of single molecule magnets have shown excellent agreement with experiment.[17,18] The Fe_8Br_8 system has, however, been a consistent challenge.[19] The disagreement between theory and experiment for this important test case may originate from an inadequate description of the electronic interaction of the *d* electrons within DFT. For instance, while we find the theoretically calculated (spin-forbidden) gap between highest occupied and lowest unoccupied molecular orbitals (HOMO-LUMO) of $[Fe_8O_2(OH)_{12}(C_6H_{15}N_3)_6Br_6]^{2+}$ is 0.15 eV, the experimentally measured transport gap of Fe_8Br_8 semiconductor is 1.4 eV.[20] If the transport gap is representative of the smallest gap in the problem, the difference between theory and experiment would be large even considering the fact that density functional theory tends to underestimate the gap. Therefore, we have endeavored to learn more about the low-lying excitations in this molecule-based magnet by comparing our electronic structure results for the isolated cluster with the polarized optical conductivity spectra of Fe_8Br_8.

The octanuclear iron(III) Fe_8-cluster (Fig. 1) has the chemical formula $[Fe_8O_2(OH)_{12}(tacn)_6]^{8+}$, with tacn $=1,4,7$-trizacyclononane $(C_6N_3H_{15})$. The approximate D_2 symmetry observed in the molecule,[3] is formally broken by the presence of halide atoms and waters of crystallization. The central iron atoms are connected by oxo-hydroxo bridges. The Fe(III) ions have a d^5 electron configuration. The ferrimagnetic coupling of spins between the eight Fe atoms results in an $S=10$ spin ground state.[21] The organic tacn-rings are very important for stabilizing the magnetic core of the molecule because the three lone pairs of nitrogen complete a quasi sixfold environment for the Fe atoms. Further, the tacn rings separate the Fe_8-clusters in the crystal, resulting in negligible intermolecular dipole fields, typically on the order of 0.05 T (See Ref. 8). The resulting formal charge states are nominally Fe^{3+}, $(OH)^{-1}$, O^{-2}, and $tacn^0$, leading to a molecule with an overall formal charge state of +8 which may then be compensated by the eight negatively charged halide ions. The $[Fe_8O_2(OH)_{12}(tacn)_6]^{8+}$ molecule is the building block of the $[(C_6H_{15}N_3)_6Fe_8(\mu_3-O)_2(\mu_2-OH)_{12}]Br_7(H_2O)Br.8H_2O$ molecular crystal.

We have also studied the electronic and magnetic structure of $FeCl_3$-(tacn) molecule, which occurs as a precursor to Fe_8Br_8 in the synthetic process. In this molecule, the Fe is in sixfold coordination with three Cl ions and the three nitrogens from the tacn ring. The $[FeCl_3$-(tacn)] molecule has C_3 symmetry, as evident from Fig. 2. Note that the coordination of the Fe atoms in this complex is similar to that in the Fe_8Br_8 molecule, making $[FeCl_3$-(tacn)] an important model compound for assessing the electronic structure and optical spectra of the title material.

In Secs. II and III, we give information about computational details and discuss the experimental method. A discussion of the results is presented in Sec. IV followed by the conclusions in Sec. V.

II. COMPUTATIONAL DETAILS

The initial geometry of the $Fe_8Br_6^{2+}$ molecule was generated from the x-ray scattering data deposited at the Cambridge Crystallographic Data Center (Cambridge, UK).[3] The Fe_8Br_8 cluster has a total of 186 atoms without counting the water molecules of crystallization, putting it in a size regime that is still a challenge for density-functional calculations at the all-electron level. Our previous experience with the Fe_8Br_8 cluster shows that all-electron calculations are the most reliable way to obtain the electronic structure of this

cluster.[19] Our group's earlier calculation on the Fe_8Br_8 molecule, carried out by adopting a geometry with a different number of forced symmetry operations, raised questions about the electronic density of states within 0.5 eV of the Fermi level[19] and suggested that the magnetic anisotropy energy is strongly dependent upon the electronic states and energies in this region. The calculations of Ref. 19 both with Br ions and Br replaced by F ions and those presented here show a common attribute which we believe is indicative of the underlying question related to the electronic structure. Accounting for the precise charge transfer between the halide anions and the Fe cations is exceedingly important in this compound. Bromine NMR measurements showing small amounts of spin density on the Br counteranions also point to the sensitivity of the material to these issues and raise the possibility that incomplete Br-to-Fe charge transfer may occur.[22]

In the molecular crystal, the positively (+8) charged Fe_8-cluster is neutralized by eight Br ions. However, when the two symmetry-breaking Br^- ions are removed, the remaining structure has only inversion symmetry. Here, we have adopted an isolated Fe_8^{2+} geometry with the inversion symmetry, which leads to a 184-atom $[Fe_8Br_6]^{2+}$ complex with 92 inequivalent atoms. In the actual crystal, the halide ions break this symmetry. The magnetic core, with iron and the oxo-hydroxo bridges, is unchanged by our chosen symmetry operations. It should be noted that treating the $Fe_8Br_6^{2+}$ analog leads to a system with complete Br-to-Fe charge transfer and a nonzero HOMO-LUMO gap. Once a gap is obtained in the system, the geometry optimization is readily accomplished.

The DFT calculations[16] discussed herein were performed at the all-electron level with Gaussian-orbital-based NRLMOL program.[23] All calculations employed the Perdew-Burke-Ernzerhof generalized-gradient approximation (GGA) for the density-functional.[24] NRLMOL combines large Gaussian orbital basis sets, numerically precise integration, and an analytic solution of Poisson's equation in order to accurately determine the self-consistent potentials, secular matrix, total energies, and Hellmann-Feynman-Pulay forces.[25] The exponents for the single Gaussians have been fully optimized for DFT calculations.[26]

To coax the system toward ferrimagnetic spin-ordering, we follow the same method as used in Ref. 17 and start our calculations with overlapping atomic potentials. To allow for the possibility of spin ordering, we add to this potential an empirical starting potential which favors the spin-ordering shown in Fig. 1. After the first iteration, this potential is removed and all the electronic and spin degrees of freedom are optimized variationally. The system may either accept or reject the ferrimagnetic ordering, depending upon the relative energetics of the spin ordering. The geometry of the cluster was optimized till forces on all atoms dropped below 0.002 a.u. The spin-ordering was found to be ferrimagnetic, with $S=10$, in accord with experiment. The basis set employed in this calculation consisted of 1262 contracted Gaussians, optimized for each atom. Basis set details are summarized in Table I. A variational mesh was employed for the numerical integrations.[23]

The optical absorption spectrum for the $Fe_8Br_6^{2+}$ molecule was calculated using the dipole matrix elements (length formulation) and a reasonable broadening factor similar to that discussed in Ref. 27. Because we determine the dipole matrix elements using a length rather than velocity formulation, a prefactor of E^2 is included to account for the known relationship between the dipole and length forms, where E is the eigenvalue difference of the states in consideration. By comparing the simulated spectrum of the building-block molecule with the experimental optical spectrum of the molecular solid, we can assess the electronic structure of $[(C_6H_{15}N_3)_6Fe_8(\mu_3\text{-}O)_2(\mu_2\text{-}OH)_{12}]Br_7(H_2O)Br.8H_2O$.

TABLE I. The maximum and minimum exponents of the bare Gaussians, the number of bare Gaussians, and the number of contracted Gaussians for each angular momentum for different atoms used in the calculation of $Fe_8Br_6^{2+}$.

Atom	α_{max}	α_{min}	N_{bare}	*s p d*
H	77.84	0.0745	6	2 1 1
C	2.2×10^4	0.0772	12	3 2 1
N	5.1×10^4	0.0941	13	3 2 1
O	6.1×10^4	0.1049	13	3 2 1
Fe	3.8×10^6	0.0452	20	5 3 2
Br	7.9×10^6	0.0781	21	5 4 2

III. EXPERIMENTAL METHODS

A. Crystal growth

Single crystals of $[(C_6H_{15}N_3)_6Fe_8(\mu_3\text{-}O)_2(\mu_2\text{-}OH)_{12}]\times Br_7(H_2O)Br.8H_2O$ were synthesized using the procedure of Wieghardt *et al.*[3] and slow evaporation techniques. Typical dimensions were $\approx 1\times1\times0.5$ mm^3. The samples are routinely monitored for quality by NMR, x-ray diffraction, and magnetization measurements. Our optical measurements were made on freshly grown Fe_8Br_8 single crystals, as degradation occurred in some samples over time. Pressed powder samples of the $[FeCl_3\text{-}(tacn)]$ model compound were employed for these experiments.

B. Spectroscopic measurements

Near normal polarized reflectance measurements were carried out over a wide energy range (4.5 meV–5.5 eV, 35–45 000 cm^{-1}) using a series of different spectrometers including a Bruker 113V Fourier transform infrared spectrometer, a Bruker Equinox 55 equipped with an infrared microscope, and a Perkin Elmer Lambda-900 grating instrument. The spectral resolution was 2 cm^{-1} in the far and middle infrared and 2 nm in the near-infrared, visible, and near-ultraviolet. All data were collected at 300 K. Various wire grid, film, and crystal polarizers and analyzers were employed as appropriate. We concentrated our efforts on the large (*ab*-plane) crystal face. The polarizers/analyzers were positioned to record spectra in the two directions of greatest optical anisotropy on this face, corresponding to the *b* and $\perp b$ directions, respectively. Small off-diagonal dielectric terms are certainly anticipated for low symmetry crystals such as Fe_8Br_8; our choice of polarizer/analyzer configura-

tion minumizes this effect. A Kramers-Kronig analysis was used to calculate the optical conductivity from the measured reflectance, yielding information on the lossy response of the material.[28] Standard peak-fitting techniques were used, where appropriate.

IV. RESULTS AND DISCUSSION

A. Probing the electronic structure of the $Fe_8Br_6^{2+}$ molecule and the molecular solid

We first note that the experimentally observed spin ordering[21,29] is well reproduced in our calculations. This is an important issue for the Fe_8Br_8 molecule since our calculations on a similar complex with 7 Br^- ions show that the spin ordering depends on the number of Br ions and the geometry.[30] The spin density of the $[Fe_8O_2(OH)_{12}(C_6H_{15}N_3)_6Br_6]^{2+}$ is shown in Fig. 1. Spin density isosurfaces of both signs are seen on Fe sites as well as the bridging oxygen atoms, indicative of ferrimagnetic ordering. Experiments by Pontillon *et al.*[29] and Furukawa *et al.*[31] confirm not only the ferrimagnetic ordering but find smaller local moments on the two minority-spin Fe atoms than on the six majority-spin Fe sites. In order to ascertain changes in the local moments as a function of atom type, we placed a sphere of 2.19 bohr around each Fe and calculated the net moment inside each sphere. For the two iron atoms with opposite spins, we obtain a moment of 3.42 μ_B, whereas the six ferromagnetically aligned irons have moments ranging from 3.74 to 3.85 μ_B, which is in qualitative accord with experiment. As discussed in the next section, the corresponding local moment for the $S=5/2$ $FeCl_3$-tacn molecule is 3.83 μ_B. This suggests that the antiparallel-ordered Fe atoms have qualitatively lower moments than those associated with more standard $S=5/2$ Fe ions. For further comparison, we note that in Mn_{12}-acetate, the nominally $S=2$ and $S=3/2$ Mn ions are found to have local moments of 3.6 and 2.7 μ_B within a sphere of 2.5 bohr. After considering all of the calculated data on local moments, we suggest that the calculated local moments in the Fe_8Br_8 compound are indicative of six $S=5/2$ majority spin Fe sites and two minority spin Fe atoms that are somewhere between $S=2$ and $S=5/2$.

Figures 3 and 4 display the calculated total and atom-projected spin-majority and spin-minority density of states for $[Fe_8O_2(OH)_{12}(C_6H_{15}N_3)_6Br_6]^{2+}$. The spin of the HOMO and LUMO are different, and there is a small 0.15 eV gap between them. The spin majority channel has a HOMO-LUMO gap of 0.54 eV. Based upon several decades of experience with the DFT method, excitation energies are generally underestimated by a typical factor of 1.4. One of the seminal discussions of the so-called "band gap" problem can be found in Ref. 32. Scaling of the majority channel gap therefore yields 0.76 eV. This is the $\Delta k=0$ transition, which should correspond to a peak in the measured optical spectrum. The states near the Fermi level are derived mainly from Fe atoms, with smaller contributions from both O, N, and C sites. In contrast to earlier calculations, which included eight (rather than six) halide anions, Br spin-up and -down states lie deep in energy. The spin minority channel

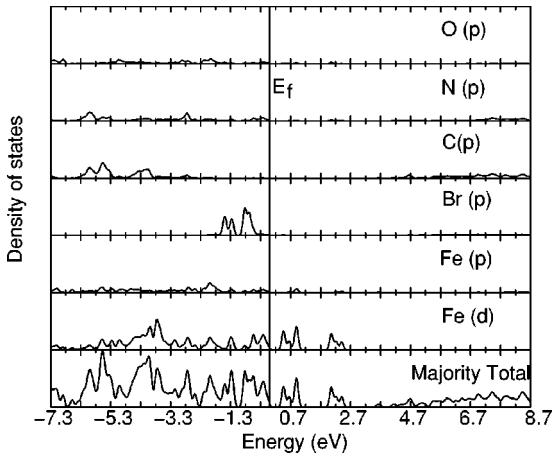

FIG. 3. Calculated density of states for majority spin electrons. E_f shows the position of the Fermi energy. The energies are scaled with respect to the position of the Fermi energy.

shows a HOMO-LUMO gap of 0.23 eV. Scaling this transition by a factor of 1.4 as before, such a feature might be expected to appear as a peak in the measured optical spectrum at ~0.32 eV. In this case, the states near the Fermi level originate mainly from Fe atoms. The modest spin density on the O and N sites leads to small spin density on the bridging O and some of the N atoms in the tacn rings. From the spin density isosurface we find that the oxygens associated with the hydroxo bridges exhibit more spin polarization than the oxygen bridges. A large number of both occupied and unoccupied states near the Fermi level originate from the Fe *d* states. The filled Br *p* states show small spin polarization compared to the Fe centers. Higher energy (unoccupied) states have large C and N *p* contributions.

Figure 5 shows the calculated optical absorption spectrum, obtained from an analysis of the dipole matrix elements of $Fe_8Br_6^{2+}$. The two projections correspond to the two polarizations along which the optical response was measured. Experimentally, these directions were chosen to maximize the anisotropy in the *ab*-plane optical properties, thus

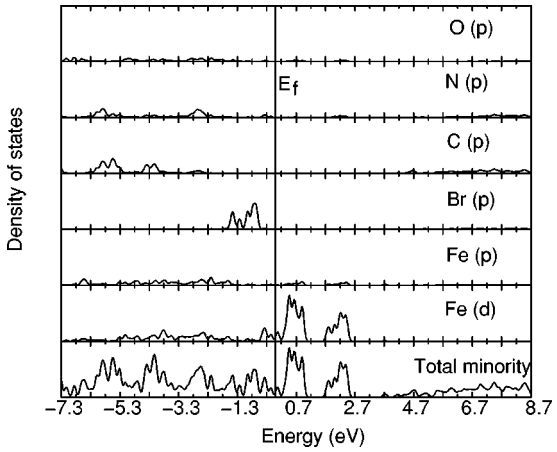

FIG. 4. Calculated density of states for minority spin electrons. E_f shows the position of the Fermi energy. The energy scale is given with respect to the position of the Fermi energy.

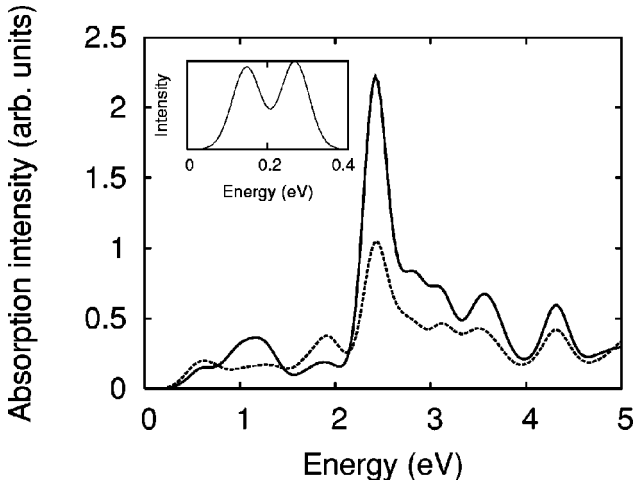

FIG. 5. Spin-averaged joint density of states for Fe_8Br_8 weighted by the dipole matrix elements. The theoretical curves are broadened by a Gaussian, with full width half maximum of 0.27 eV, to simulate a realistic spectrum. The solid (dashed) curves show the simulated spectra in the $\|b$ ($\perp b$) directions. The inset shows the low energy excitations seen after inclusion of spin-orbit coupling (see text).

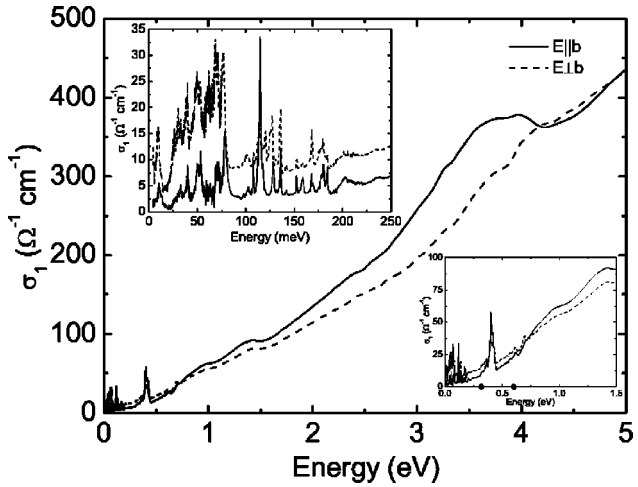

FIG. 6. Polarized optical conductivity of the $[(C_6H_{15}N_3)_6Fe_8(\nu_3-O)_2(\mu_2-OH)_{12}]Br_7(H_2O)Br.8H_2O$ molecular magnet at 300 K. The upper inset shows a magnified view of the infrared region. The lower inset displays a close-up view of the rising edge of the optical conductivity. The experimental values of the spin forbidden HOMO-LUMO (see text) and majority optical gap are indicated by filled circles on the baseline in this panel; $2\Delta_{opt}=0.3$ eV and $2\Delta_{opt,maj}=0.6$ eV. Overall, we find that the low-energy features are dominated by Fe $d\rightarrow$Fe d interionic excitations, whereas the higher energy features are due to O $p\rightarrow$Fe d charge transfer transitions.

assuring that they correspond to the principal axes of the dielectric tensor.[33]

Figure 6 displays the 300 K polarized optical conductivity of $[(C_6H_{15}N_3)_6Fe_8(\mu_3\text{-}O)_2(\mu_2\text{-}OH)_{12}]Br_7(H_2O)Br.8H_2O$. The response is that of a semiconductor, with modest spectral anisotropy. Based upon a comparison of the measured optical conductivity with the calculated dipole weighted joint density of states, we assign the peak at ~0.9 eV as the theoretical 0.54 eV HOMO-LUMO gap in the majority spin channel. When empirically scaled by an appropriate factor of 1.4, the agreement between the calculated (0.76 eV) and measured (~0.9 eV) features is quite good. The calculated minority HOMO-LUMO gap is 0.23 eV. When appropriately scaled, this corresponds to 0.32 eV, a reasonable match with a rather broad low-energy feature (centered at ~0.4 eV) in the experimental spectrum. However, electronic dipolar transitions between these states are forbidden by symmetry in the $Fe_8Br_6^{2+}$ system. The other candidate is the 0.15 eV HOMO-LUMO gap (with a scaled value of 0.21 eV), although as previously mentioned, the spin channels are different. Our assignment and current understanding of this low-energy spectral feature will be discussed in detail below. From the experimental point of view, the optical gap is typically determined by a linear extrapolation of the leading edge of the absorption band down to the baseline. Such an analysis yields optical gaps of ~0.3 and 0.6 eV, which we assign as majority to minority HOMO-LUMO and majority gaps, respectively. We consider the overall agreement between theory and experiment to be excellent, considering that the experiments are done on a crystalline sample and the DFT calculations (which typically underestimate band gaps and excitation energies) are carried out on a single molecule.

The transport gap is substantially larger, 1.46 eV.[20] This difference suggests that the transport gap may be mediated by many larger energy excitations rather than a few low-energy excitations. Alternatively, the transport gap may arise from a barrier encountered by electrons hopping between two neighboring molecules. Motivated by the connection between charge transfer and hopping-related transport, we note that extrapolation of the leading edge of the absorption band centered at 3.5 eV in the experimental spectrum (Fig. 6) yields a value of ~1.5 eV. The magnitude of the optical conductivity is also more substantial above 1.5 eV and con-

TABLE II. Comparison of the gap values obtained from theoretical calculation, optical conductivity experiments, and transport measurements. Theoretically, the spin minority gap is dipole forbidden. Inclusion of spin-orbit coupling activates the 0.15 eV HOMO-LUMO gap, which is otherwise spin forbidden. The experimental spectrum shows a low-energy gap at 0.3±0.1 eV (with the peak at ~0.4 eV), the assignment of which is discussed in the text. All values are in electron volts.

$2\Delta_{H-L}$ (Theory)	$2\Delta_{Min}$ (Theory)	$2\Delta_{Maj}$ (Theory)	$2\Delta_{Maj/Min}$ (Expt)	$2\Delta_{Maj}$ (Expt)	$2\Delta_{Trans}$ (Expt)	Technique
$0.15\times1.4=0.21$	$0.23\times1.4=0.32$	$0.54\times1.4=0.76$				DFT, this work
~0.4 Peak		~0.9 Peak	0.3±0.1	0.6±0.1	1.5±0.2	Optics, this work
					1.46±0.2	Transport, Ref. 20

sequently seems to define the energy scale for charge transport in Fe_8Br_8. Interestingly, the transport gap in Mn_{12}-acetate compares well with the measured optical gap.[20,34] A comparison of the theoretical, optical, and transport gaps for the Fe_8Br_8 system is given in Table II.

Based upon an analysis of the minority- and majority-channel density of states and a comparison of the calculated joint density of states with the optical experimental spectrum, we make the following assignments of the observed electronic excitations in the molecular solid. The 0.5 eV peak in the theoretical curve (Fig. 5) arises from Fe $d \rightarrow$ Fe d interionic excitations. That is, they arise from electronic excitations involving an occupied electron being moved to a hole on a neighboring antiferromagnetically coupled Fe ion. The 1.2 eV feature arises from a combination of Fe $d \rightarrow$ Fe d and Br $p \rightarrow$ Fe d transitions. The 1.8 eV peak is due to Br and O $p \rightarrow$ Fe d as well as Fe $d \rightarrow$ Fe d transitions. The predicted features near 0.5 eV, between 1.1 and 1.3 eV, and at 1.8 eV in the theoretical curve correspond to the peaks at ~0.9, 1.4, and 2.3 eV in the experimental optical conductivity spectrum. Theoretical calculations predict that the two spectra cross near 1.6 and 2.2 eV, whereas crossing of the $\|b$ and $\perp b$ spectra is observed near 0.75 and 4.2 eV in Fig. 6. The theoretical joint density of states (Fig. 5) shows maximum anisotropy near 2.4 eV. Appropriately scaled, this feature is a good match with the experimental peak centered at 3.5 eV. We note that the 3.5 eV feature (Fig. 6) displays substantial directional dependence, in agreement with the calculation. We assign this structure as O $p \rightarrow$ Fe d charge transfer, with smaller contributions from Br p and Fe $d \rightarrow$ Fe d states. The peaks higher in energy arise primarily from O $p \rightarrow$ Fe d transitions.

The upper inset of Fig. 6 displays a close-up view of the infrared vibrational properties of [(C6H15N3)6Fe8(μ3-O)2(μ2-OH)12]Br7(H2O)Br.8H2O. We assign the general characteristics of these features according to our dynamics simulations[35] on the isolated molecule as well as spectral comparisons with model compounds such as $FeCl_3$(tacn). The features below 20 meV are assigned as low-energy wagging and rocking of the magnetic oxide core and free Br^- motion. Structure between 22 and 35 meV corresponds to Fe—O core wagging, rocking, twisting, and bending, in addition to free Br^- motion. Wagging and bending of the tacn ligand is observed between 35 and 42 meV. We assign the complex features between 43 and 82 meV as N—Fe—N, N—Fe—O, Fe—N—C, O—Fe—O, and Fe—O—Fe bending and twisting motion. Fe—O—Fe wagging and asymmetric stretching is observed near 117 meV. Symmetric stretching of the O—Fe—O and N—Fe—N moieties appear at slightly higher energy. Most of the features between 99 and 142 meV are related to the tacn ligand. Here, the ligand features are relatively unpolarized, whereas Fe—O motion is slightly polarized, on account of the disk-like shape of the building block molecule. These values are in good agreement with recent Raman data of North et al.[36] Ligand (tacn) motion accounts for the small features between 150 and 180 meV. Well-known C—H, O—H, and N—H symmetric stretching appear at ~360,395, and 410 meV. The latter features are quite strong, and as mentioned previously, seem to be superimposed upon a weak, low-energy electronic background. We discuss the likely origin of this electronic feature below.

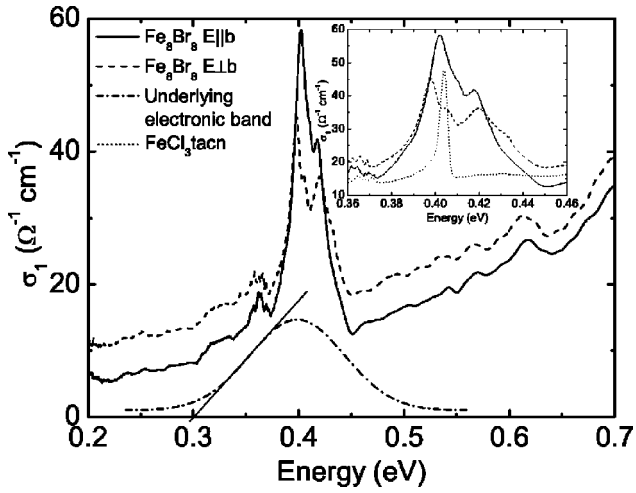

FIG. 7. Close-up view of the 300 K optical conductivity of Fe_8Br_8 in the b and $\perp b$ directions. The weak underlying low-energy electronic excitation was fit using a model oscillator and is drawn as a guide to the eye (dash-dotted line). C—H, O—H, and N—H vibrational modes are superimposed upon this structure. The straight solid line illustrates optical gap determination for this feature. The inset compares the unpolarized vibrational response of the [$FeCl_3$-(tacn)] model compound with the polarized optical conductivity spectrum of Fe_8Br_8 molecular magnet.

To further understand what the electronic structure can tell us about the local moments on the minority spin Fe atoms, we discuss the lowest minority-to-minority HOMO-LUMO gap in the calculation. We predict this excitation at 0.23 eV. Empirical scaling ($\times 1.4$) raises this value to 0.32 eV. The dipole matrix element between the HOMO and LUMO state is, however, calculated to be zero. A decomposition of the HOMO and LUMO states onto the minority spin Fe atoms shows that both the HOMO and LUMO states are primarily composed of Fe 3d electrons. This constituency explains why the calculated dipole matrix element is almost exactly zero. That is, the charge-transfer portion of the dipole matrix element is null because the two minority spin Fe atoms are well separated. The onsite contribution is also predicted to be zero since these contributions have the same parity. We note that the above analysis of the LUMO level, and the dipole selection rules also supports our calculated local moments showing reduced moments on the minority spin Fe sites.

Interestingly, the optical conductivity spectrum of Fe_8Br_8 displays a weak low-energy electronic feature centered at ~0.4 eV, energetically coincident with the calculated position of the minority spin gap (0.32 eV). A close-up view of the measured optical response is shown in Fig. 7; the dash-dotted line centered near 0.4 eV illustrates the underlying electronic excitation and is a guide to the eye. In view of the formal dipole-forbidden character of the spin minority gap transition, this broad peak may correspond to the aforementioned spin minority gap (perhaps activated by the symmetry breaking Br ions in the crystal structure), a phonon-assisted

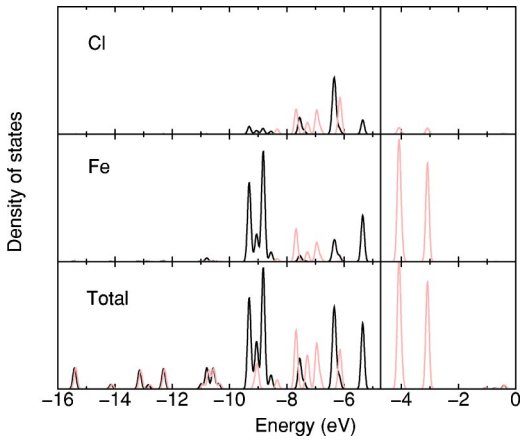

FIG. 8. Density of states for [$FeCl_3$-(tacn)]. The majority DOS is plotted in black and minority DOS is plotted in gray.

transition, or a spin-forbidden excitation (such as the spin majority to minority HOMO-LUMO gap). Well-known C—H, O—H, and N—H vibrational modes are superimposed upon this weak electronic processes. To understand the broad, low-energy spectral feature better, we have carried out a similar analysis of the optical spectra of the model [FeCl3-(tacn)] compound which is chemically similar to Fe_8Br_8 molecule. In the next section, we present our results on the model compound for which low energy electronic excitations are absent. Further, we explore the possibility that this weak, low-energy spectral feature can be attributed to the superposition of vibrational structure and a spin majority to spin minority HOMO-LUMO excitation, activated by spin-orbit coupling.

B. Understanding the electronic structure of [$FeCl_3$-(tacn)] model compound

Our interest in [$FeCl_3$-(tacn)] is primarily motivated by the chemical similarity between this model compound and the title material. Comparison of the spectral response therefore provides an important test of our assignments and understanding of the low-energy electronic structure in $[(C_6H_{15}N_3)_6Fe_8(\mu_3\text{-}O)_2(\mu_2\text{-}OH)_{12}]Br_7(H_2O)Br.8H_2O$. Before presenting the experimental results, we give a brief description of the calculated electronic structure of the [$FeCl_3$-(tacn)] molecule (Fig. 2) with a single Fe(III) center and a total spin of $S=5/2$. Similar to the $[Fe_8O_2(OH)_{12}(C_6H_{15}N_3)_6Br_6]^{2+}$ complex, the HOMO and LUMO are of different spin, with a gap of 1.26 eV. The calculated majority and minority spin gaps are 4.29 and 2.01 eV respectively. The calculated density of states (Fig. 8) shows large contributions from Fe *d* and the Cl *p* states in the occupied region whereas the unoccupied states arise mostly from the Fe *d* states. The spin minority HOMO and the LUMO have strong Cl *p* and Fe *d* character, respectively. The isotropic dipole-weighted joint density of states for [$FeCl_3$-(tacn)] is shown in Fig. 9. The most dominant excitations are the Cl $p \rightarrow$ Fe *d* transitions with a small contribution from N $p \rightarrow$ Fe *d* transitions. There is, however, no similarity between the predicted spectra of the

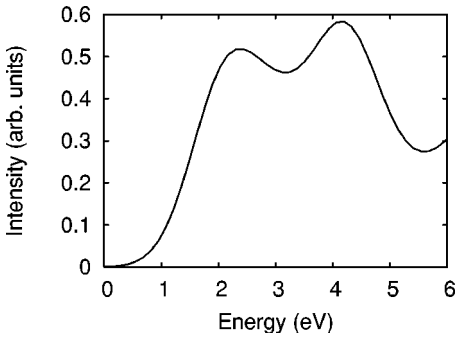

FIG. 9. Calculated optical absorption spectrum for the [FeCl3-(tacn)] molecule.

$[Fe_8O_2(OH)_{12}(C_6H_{15}N_3)_6Br_6]^{2+}$ and the model compound [$FeCl_3$-(tacn)] in the low-energy region. In particular, the HOMO-LUMO gap in $[Fe_8O_2(OH)_{12}(C_6H_{15}N_3)_6Br_6]^{2+}$ is an order of magnitude smaller than that in [$FeCl_3$-(tacn)]. Thus, no electronic excitations are expected below 1 eV in [FeCl3-(tacn)]; any observed features below 1 eV in the model compound should be vibrational in nature.

Revisiting the optical conductivity spectrum of the $[(C_6H_{15}N_3)_6Fe_8(\mu_3\text{-}O)_2(\mu_2\text{-}OH)_{12}]Br_7(H_2O)Br.8H_2O$ molecular magnet, we discuss the weak low-energy electonic excitation underlying the well-known C—H, O—H, and N—H vibrational features near 0.4 eV. The inset of Fig. 7 compares the vibrational properties of the molecular magnet with those of the [$FeCl_3$-(tacn)] model compound. These intramolecular vibrational modes are sharp and well-defined in the model compound, different from the broad peak shape over the same energy range for Fe_8Br_8. Two possible origins for the broad low-energy peak shape are considered. (1) That Fe_8Br_8 has a much more complicated atomic structure than the [$FeCl_3$-(tacn)] model compound and therefore may have a much larger number of vibrational modes involving C—H, N—H, O—H stretching with slightly different frequencies as well as possible low energy modes involving the Fe ions. The large number of modes due to the slightly different local symmetry could bring about the observed broadening of the peak shapes. (2) The broad structure in the spectrum of the Fe_8Br_8 molecule-based magnet may be attributable to a low-energy electronic structure, with superimposed vibrational modes. Since investigation of the first possibility is computationally very expensive for a large molecule like Fe_8Br_8, we explore the second possibility in greater detail below.

Since the transition across the spin minority gap is dipole forbidden, one possible explanation for a low energy peak in the measured spectrum could be an admixing of the Fe *p* and *d* states in the unoccupied region due to spin-orbit coupling. We have carried out a simple analysis of the dipole matrix elements obtained after inclusion of spin-orbit coupling. We find that in the region below 0.3 eV, two low intensity excitations occur at 0.27 and 0.14 eV (inset, Fig. 5). The intensity and the position of these excitations vary depending on the direction of magnetization, by about 40% and 2%, respectively. These excitations, activated by spin-orbit coupling, are from the HOMO and another high energy occupied state near Fermi level to the lowest unoccupied state. An analysis of these states show that the occupied states are

about 98% spin majority, whereas the unoccupied state is about 98% spin minority. These excitations are of low intensity and are intramolecular in nature. The spin majority to minority character of the transition is also consistent with low intensity. Such weak intramolecular transitions are not likely to contribute to the transport, where the important excitations are intermolecular in nature. This result may, in part, explain the large gap observed in transport experiments.[20] We also note that various symmetry-breaking mechanisms might activate the spin minority HOMO-LUMO gap. For instance, inclusion of the two inversion symmetry breaking Br^- ions in our calculation may change the selection rules. Another possible mechanism for activation of dipolar transitions in the low energy region can be coupling of a phonon to the electronic excitation. Calculations of such phonon assisted transitions are, however, beyond the scope of the present work.

V. SUMMARY

In conclusion, we report the electronic structure and optical properties of the $[Fe_8O_2(OH)_{12}(C_6H_{15}N_3)_6Br_6]^{2+}$ molecule using an all-electron DFT formalism, and we compare the results with the experimentally measured optical conductivity spectrum of the $[(C_6H_{15}N_3)_6Fe_8(\mu_3\text{-}O)_2(\mu_2\text{-}OH)_{12}]Br_7(H_2O)Br.8H_2O$ molecule-based magnet. The agreement is excellent. We find that interionic Fe $d \rightarrow d$ excitations dominate the spectrum in the low energy region, whereas O $p \rightarrow$ Fe d transitions dominate the high energy region. The contributions from Br p states are also significant. The observed modest optical anisotropy is well reproduced by our calculation. We suggest that the 0.4 eV peak in the optical conductivity may be attributable to the spin majority to minority HOMO-LUMO excitation, activated by inclusion of spin-orbit coupling, which mixes states of different symmetry and spin. C—H, N—H, and O—H stretching motion is present and superimposed. While the theoretical majority spin gap and the corresponding peak position (and the extrapolated gap) obtained from optical conductivity are in agreement, the transport gap is larger, indicating that high energy excitations or an intermolecular hopping barrier is involved in the electron transport.

We find that for $[Fe_8O_2(OH)_{12}(C_6H_{15}N_3)_6Br_6]^{2+}$, density functional theory with the present parametrization of GGA (Ref. 24) functional describes the electronic structure of the molecular solid well, as evidenced by our detailed comparison of the calculated optical spectrum with experiment, although the HOMO-LUMO gaps are consistently underestimated. Underestimation of the gap can also affect the calculated magnetic properties. This is a known problem with most parametrizations of the exchange-correlation functionals used in DFT and can be partly rectified by inclusion of self-interaction correction. Further work is in progress in this direction.

ACKNOWLEDGMENTS

This work was supported at NRL by ONR (Grant No. N000140211046) and the DoD CHSSI initiative administered by HPCMO, at the University of Tennessee by the Petroleum Research Fund (Grant No. PRF-AC 38164) administered by the American Chemical Society, and at Florida State University by the National Science Foundation (Grant No. DMR 0103290).

[1] T. Lis, Acta Crystallogr., Sect. B: Struct. Crystallogr. Cryst. Chem. **36**, 2042 (1980).
[2] J. Friedman, M. P. Sarachik, J. Tejeda, J. Maciejewski, and R. Ziolo, Phys. Rev. Lett. **76**, 3820 (1996); L. Thomas, F. Lionti, R. Ballou, D. Gatteschi, R. Sessoli, and B. Barbara, Nature (London) **383**, 145 (1996).
[3] K. Wieghardt, K. Pohl, I. Jibril, and G. Huttner, Angew. Chem., Int. Ed. Engl. **23**, 77 (1984); Cambridge Crystallographic Data Centre; Refcode: COCNAJ; http://www.ccdc.cam.ac. uk/
[4] A.-L. Barra, P. Brunner, D. Gatteschi, Ch. E. Schulz, and R. Sessoli, Europhys. Lett. **35**, 133 (1996).
[5] L. Thomas, F. Lionti, R. Ballou, D. Gatteschi, R. Sessoli, and B. Barbara, Nature (London) **383**, 145 (1996); J. A. A. J. Perenboom, J. S. Brooks, S. Hill, T. Hathaway, and N. S. Dalal, Phys. Rev. B **58**, 330 (1998).
[6] C. Sangregorio, T. Ohm, C. Paulsen, R. Sessoli, and D. Gatteschi, Phys. Rev. Lett. **78**, 4645 (1997).
[7] W. Wernsdorfer and R. Sessoli, Science **284**, 133 (1999).
[8] W. Wernsdorfer, T. Ohm, C. Sangregorio, R. Sessoli, D. Mailly, and C. Paulsen, Phys. Rev. Lett. **82**, 3903 (1999).
[9] F. Fominaya, P. Gandit, G. Gaudin, J. Chaussy, R. Sessoli, and C. Sangregorio, J. Magn. Magn. Mater. **195**, L253 (1999).
[10] W. Wernsdorfer, T. Ohm, C. Sangregorio, R. Sessoli, D. Mailly, and C. Paulsen, Phys. Rev. Lett. **82**, 3903 (1999).
[11] E. del Barco, N. Vernier, J. M. Hernandez, J. Tejada, E. M. Chudnovsky, E. Molins, and G. Bellessa, Europhys. Lett. **47**, 722 (1999); E. del Barco, J. M. Hernandez, J. Tejada, N. Biskup, R. Achey, I. Rutel, N. Dalal, and J. Brooks, Phys. Rev. B **62**, 3018 (2000).
[12] W. Wernsdorfer, A. Caneschi, R. Sessoli, D. Gatteschi, A. Cornia, V. Villar, and C. Paulsen, Phys. Rev. Lett. **84**, 2965 (2000).
[13] X. X. Zhang, H. L. Wei, Z. Q. Zhang, and L. Zhang, Phys. Rev. Lett. **87**, 157203 (2001).
[14] K. Park, M. A. Novotny, N. S. Dalal, S. Hill, and P. A. Rikvold, Phys. Rev. B **65**, 014426 (2002); S. Hill, S. Maccagnano, K. Park, R. M. Achey, J. M. North, and N. S. Dalal, *ibid.* **65**, 224410 (2002); S. Hill, R. S. Edwards, S. I. Jones, N. S. Dalal, and J. M. North, Phys. Rev. Lett. **90**, 217204 (2003); S. Hill, J. A. A. J. Perenboom, N. S. Dalal, T. Hathaway, T. Stalcup, and J. S. Brooks, *ibid.* **80**, 2453 (1998).
[15] L. Cianchi, F. Giallo, G. Spina, W. Reiff, and A. Caneschi, Phys. Rev. B **65**, 064415 (2002).
[16] P. Hohenberg and W. Kohn, Phys. Rev. **136**, B864 (1964); W. Kohn and L. J. Sham, Phys. Rev. **140**, A1133 (1965).
[17] M. R. Pederson and S. N. Khanna, Phys. Rev. B **60**, 9566 (1999).
[18] J. Kortus, M. R. Pederson, T. Baruah, N. Bernstein, and C. S.

Hellberg, Polyhedron, Int. J. Inorg. Org. Chem. **22**, 1871 (2003).
[19] J. Kortus, M. R. Pederson, C. S. Hellberg, and S. N. Khanna, Eur. Phys. J. D **16**, 177 (2001); M. R. Pederson, J. Kortus, and S. N. Khanna, J. Appl. Phys. **91**, 7149 (2002).
[20] J. M. North, D. Zipse, N. S. Dalal, E. S. Choi, E. Jobiliong, J. S. Brooks, and D. L. Eaton, Phys. Rev. B **67**, 174407 (2003).
[21] R. Caciuffo, G. Amoretti, A. Murani, R. Sessoli, A. Caneschi, and D. Gatteschi, Phys. Rev. Lett. **81**, 4744 (1998).
[22] D. Zipse, J. M. North, R. M. Achey, N. S. Dalal, S. Hill, R. S. Edwards, E. Choi, and J. S. Brooks, J. Appl. Phys. **95**, 6900 (2004).
[23] M. R. Pederson and K. A. Jackson, Phys. Rev. B **41**, 7453 (1990); K. A. Jackson and M. R. Pederson, *ibid.* **42**, 3276 (1990).
[24] J. P. Perdew, K. Burke, and M. Ernzerhof, Phys. Rev. Lett. **77**, 3865 (1996).
[25] H. Hellmann, *Einführung in die Quantentheorie* (Deuticke, Leipzig 1937); R. P. Feynman, Phys. Rev. **56**, 340 (1939); P. Pulay, Mol. Phys. **17**, 197 (1969).
[26] D. Porezag and M. R. Pederson, Phys. Rev. A **60**, 2840 (1999).
[27] W. Y. Ching, Y. N. Xu, and K. W. Wong, Phys. Rev. B **40**, 7684 (1989).
[28] F. Wooten, *Optical Properties of Solids* (Academic Press, New York, 1972).
[29] Y. Pontillon, A. Caneschi, D. Gatteschi, R. Sessoli, E. Ressouche, J. Schweizer, and E. Lelievre-Berna, J. Am. Chem. Soc. **121**, 5342 (1999).
[30] T. Baruah, J. Kortus, and M. R. Pederson (unpublished).
[31] Y. Furukawa, S. Kawakami, K. Kamagai, S-H. Beck, and F. Borsa, Phys. Rev. B **68**, 180405(R) (2003).
[32] L. J. Sham and M. Schluter, Phys. Rev. B **32**, 3883 (1985).
[33] We have confirmed that these also correspond to two eigenvectors of the calculated bare polarizability tensor in this plane.
[34] S. M. Oppenheimer, A. B. Sushkov, J. L. Musfeldt, R. M. Achey, and N. S. Dalal, Phys. Rev. B **65**, 054419 (2002).
[35] We simulated the dynamics of Fe_8Br_8 using the commercially available program TITAN. Because the title material is a molecular solid, the calculations were carried out on the isolated building block units.
[36] J. M. North, R. M. Achey, and N. S. Dalal, Phys. Rev. B **66**, 174437 (2002).